J|A|C|S COMMUNICATIONS

$Pb_2B_5O_9I$: An Iodide Borate with Strong Second Harmonic Generation

Yi-Zhi Huang,[†] Li-Ming Wu,[†] Xin-Tao Wu,[†] Long-Hua Li,[†] Ling Chen,*[,†] and Yong-Fan Zhang*[,‡]

Key Laboratory of Optoelectronic Materials Chemistry and Physics, Fujian Institute of Research on the Structure of Matter, Chinese Academy of Sciences, Fuzhou, Fujian 350002, P. R. China, and Department of Chemistry, Fuzhou University, Fuzhou, Fujian 350002, P. R. China

Received July 8, 2010; E-mail: chenl@fjirsm.ac.cn

Abstract: The combination of lone-pair effects on Pb^{2+} cations and the smaller electronegativity of I^- anions into the pentaborate framework generates a phase-matchable material, $Pb_2B_5O_9I$, with the largest powder SHG response among borates, about 13.5 times that of KDP (KH_2PO_4), and transparency over the near-UV to middle-IR region. DFT calculations on electronic structure and cutoff-energy-dependent SHG coefficients confirm these origins.

Borates have long been a remarkable source of nonlinear optical (NLO) materials,[1] and some examples, such as β-BaB_2O_4 (BBO) and LiB_3O_5 (LBO), have been commercially manufactured and used worldwide. The asymmetric electronic distributions on the distorted planar anions of $[B_3O_6]^{3-}$ and $[B_3O_7]^{5-}$ are responsible for the large second harmonic generation (SHG) in these, respectively. The design and construction of new inorganic NLO materials often utilize MO_n polyhedra as effective noncentrosymmetric (NCS) building units. These may contain second-order Jahn−Teller (SOJT) distorted cations such as d^0 transition metal ions,[2,3] *p*-cations with stereochemically active lone pairs (quoted as lone-pair effects subsequently),[4−7] or d^{10} cations with large polar displacement in a few cases.[8,9] The combination of diverse functional building units can produce materials with high NLO performance; for example, powdered $Cd_4BiO(BO_3)_3$ shows an SHG response about six times that of KH_2PO_4 (6 × KDP), representing the largest powder NLO coefficient among borates to date.[8] In such a compound, the combinations of the polar displacement of d^{10} Cd^{2+} ion, lone-pair effects on Bi^{3+}, and π-delocalization of BO_3 are believed to be the origin of the strong SHG activity. In this communication, we report the discovery of $Pb_2B_5O_9I$, a phase-matchable iodide borate with an SHG intensity measured on ground crystals approximately 13.5 times that of KDP and about twice as large as that of $Cd_4BiO(BO_3)_3$.[8]

Although lighter halide pentaborates $M_2B_5O_9X$ (M = Ca, Sr, Ba, Pb, Eu; X = Cl, Br) are known, the iodide, $Pb_2B_5O_9I$, has not been obtained because of synthetic difficulties.[10−12] The sharp increase of the SHG activity along isostructural Ca < Sr < Ba < Pb for M and Cl < Br for X suggested that the key SHG factors come from not only the lone pairs on Pb^{2+} but also the bonding of the halogen anions. Consequently, the unknown iodide pentaborate, $Pb_2B_5O_9I$, would be expected to exhibit the strongest SHG activity among $M_2B_5O_9X$. In contrast, the theoretical calculations of SHG coefficients utilizing Phillips−Van Vechten−Levine−Xue bond theory indicated that the planar BO_3 triangle is the sole functional group affecting the NLO properties of the chloride and bromide pentaborates.[10] Here, we report the synthesis of $Pb_2B_5O_9I$ and density functional theory (DFT) calculations that indicate that its remarkably large SHG intensity arises from all three components, the I^- anion, the lone $6s^2$ pair on Pb^{2+}, and the borate groups.

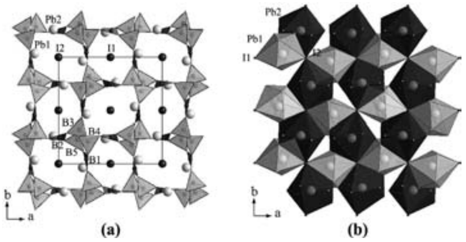

Figure 1. (a) Crystal structure of $Pb_2B_5O_9I$ viewed down *c* axis with Pb−O and Pb−I bonds omitted for clarity. Gray: BO_4 tetrahedra; black: BO_3 triangles. (b) $[Pb_2O_9I^{15-}]_n$ substructure along *c* axis. Gray and black: PbO_7I_2 monocapped hexagonal bipyramids.

Table 1. Optical Properties for $Pb_2B_5O_9X$ (X = I, Br, Cl)

	experimental		calculated	
X	SHG intensity[a]	transparent region (μm)	band gap energy (eV)[b]	SHG coefficients (pm/V)[c]
I	13.5, PM	0.40−6.96	3.33/3.36	16.6/9.4/1.8
Br	4.7, PM	0.38−6.86	3.54/3.54	7.4/2.6/−1.2
Cl	0.7, PM	0.31−6.80	3.72/3.69	4.5/1.0/−1.8

[a] Relative to KDP (150−210 μm) with $\lambda_{incident}$ = 1064 nm. PM = phase-matchable (Figure S5). [b] Direct/indirect gaps. [c] Static $d_{15}/d_{24}/d_{33}$ ($d_{15} = d_{31}$, $d_{24} = d_{32}$) according to the length-gauge formalism.[13,14]

The prismatic colorless or pale yellow $Pb_2B_5O_9I$ crystals (Figure S1) together with a second phase, brown lamellar PbB_4O_7 (ICSD 203201) were synthesized in a solid-state reaction of PbI_2/PbO/B_2O_3 in an evacuated silica tube (Supporting Information). The purity of the handpicked $Pb_2B_5O_9I$ crystals was confirmed by the XRD pattern (Figure S2a). The isostructural $Pb_2B_5O_9I$ also crystallizes in space group *Pnn*2 (No. 34).

The three-dimensional network was built from $[B_5O_9{}^{3-}]_n$ and $[Pb_2O_9I^{15-}]_n$ substructures shown in Figure 1. The primary building units in the $[B_5O_9{}^{3-}]_n$ substructure (Figure 1a) are BO_4 tetrahedra and BO_3 triangles connected in a double six-member ring motif (Figure S3a). Here the BO_4 tetrahedra form chains along the *c* axis via vertex sharing, which are further linked along both *a* (via $B2O_3$) and *b* axes (via $B1O_3$) so as to define large channels along the *c* axis. The centers of such channels are occupied by I1 or I2 anions. The $[Pb_2O_9I^{15-}]_n$ substructure is made of knitted chains of PbO_7I_2 monocapped hexagonal bipyramids via sharing I apexes along *a* and *b* axes, respectively (Figures 1b, S3b−c). The Pb1- and Pb2-polyhedron strings are condensed via shared I1−O8−O3 and I2−O4−O5 faces and I1−O7 edges (Figure S4). Compared with the earlier $Pb_2B_5O_9X$ (X = Cl, Br), the PbO_7I_2 polyhedra exhibit significantly greater distortions, such as the angle reduction for I−Pb−I (137° and 152°) with respect to Cl−Pb−Cl (157° and 163°) and Br−Pb−Br (150° and 160°) as well as the larger Pb1−O distance ranges (2.50−3.28 Å vs 2.50−2.92 Å for Cl and 2.48−3.02 Å for Br, respectively). The structure parameters indicate an enhancement of the SOJT distortion in PbO_7I_2

[†] Chinese Academy of Sciences.
[‡] Fuzhou University.

10.1021/ja106066k

polyhedra, which arises from the larger electronegativity difference between the coordinated I^- and O^{2-} anions.

The measured and calculated optical parameters for $Pb_2B_5O_9X$ (X = I, Br, Cl) are summarized in Table 1 (more details in the Supporting Information). Powdered $Pb_2B_5O_9I$ shows an SHG activity of approximately 13.5 × KDP, much greater than those of the two lighter analogues (Figure S5), a relative smaller band gap of about 3.1 eV (Figure S6a), and a similar infrared absorption edge of about 7.0 μm (Figure S6b). From Cl to I, the increasing SHG and the decreasing band gap are consistent with the calculated results. An additional calculation also indicates that the strong SHG intensity of $Pb_2B_5O_9I$ does not originate from just a reduction of the band gap. If $Pb_2B_5O_9I$ had a band gap of 3.7 eV, i.e., the calculated value for $Pb_2B_5O_9Cl$, the calculated d_{15} would decrease only to 11.1 pm/V, still significantly greater than the 4.5 pm/V for $Pb_2B_5O_9Cl$. Subsequently, the detailed electronic structures around the Fermi level (E_F) were also studied.

The densities of states (DOS) of $Pb_2B_5O_9I$ are shown in Figure 2a with assigned numbers to mark different regions in the valence bands (VB) and conduction bands (CB) for the sake of clarity. Below E_F, the B−O bonding states are dispersed from VB-5 to VB-2, and Pb 6s states mix with I 5p as well as O 2p over VB-4 to VB-1. Above E_F, the prominent characters for each region are as follows: CB-1, Pb 6p states (with small contribution of I 5p); CB-2, B−O π-antibonding states on BO_3; CB-3, I 5d states; and CB-4, B−O σ-antibonding states from both BO_3 triangles and BO_4 tetrahedra (with small I 5d contribution). The lone pairs on Pb^{2+} are characterized mainly by Pb 6s-O 2p bonding interactions at VB-4 and (Pb 6s-O 2p)-I 5p antibonding−antibonding interactions at VB-1. The high-energy VB-1 region dominated by I 5p states is responsible for the lone-pair effects on Pb^{2+}, which is visualized by the asymmetric electron distribution around the cations as shown in Figure 2b (versus the symmetric density at VB-4, Figure S7). This lone-pair effect is different from that for MO_x polyhedra (M = p metals) in which M ns usually mixes with O 2p and M np.[15−18] Obviously, the filled I 5p in $Pb_2B_5O_9I$ better matches the Pb 6s energy than does the empty Pb 6p. Furthermore, relative to $Pb_2B_5O_9Cl$ and $Pb_2B_5O_9Br$ (Figure S8), the I 5p in $Pb_2B_5O_9I$ contributes more significantly to the lone-pair effects on Pb^{2+} at VB-1 owing to the smaller electronegativity of I, and I 5d states disperse much more around the empty B−O states, in both CB-3 and CB-4, because of their strong penetration effect. Note that, from I to Cl, the B−O states in the electronic structures of $Pb_2B_5O_9X$ do not show obvious changes.

The local structure contributions of $Pb_2B_5O_9I$ to the overall SHG efficiency have been estimated by the cutoff-energy-dependent SHG coefficient according to the length-gauge formalism.[13,14] As clearly shown in Figure 2c, the states at VB-1, CB-3, and CB-4 make the most significant contributions to the SHG coefficient. Similar calculations for $Pb_2B_5O_9Br$ and $Pb_2B_5O_9Cl$ (Figure S9) show that these regions contribute much less to the overall SHG efficiencies. Since the dominant characters of VB-1, CB-3, and CB-4 regions are filled I 5p, empty I 5d, and B−O states, respectively, one may speculate that the electronic transitions from I 5p to I 5d and to B−O states are reflected in the high SHG efficiency. However, the following evidence excludes such a speculation. A hypothetical "$Ba_2B_5O_9I$" without lone pairs has been built in the same crystallographic structure of $Pb_2B_5O_9I$. The parallel calculations on "$Ba_2B_5O_9I$" generate a very small coefficient, 3.2 pm/V, which is even smaller than 4.5 pm/V for $Pb_2B_5O_9Cl$. Obviously, the main contributor in VB states should come from the lone-pair effect on Pb^{2+} at VB-1 instead of I 5p alone. Consequently, the sharp SHG increase for $Pb_2B_5O_9I$ in comparison with $Pb_2B_5O_9Br$ and $Pb_2B_5O_9Cl$ originates mainly with the increased cooperation of I^-, Pb^{2+} lone pairs and B−O groups.

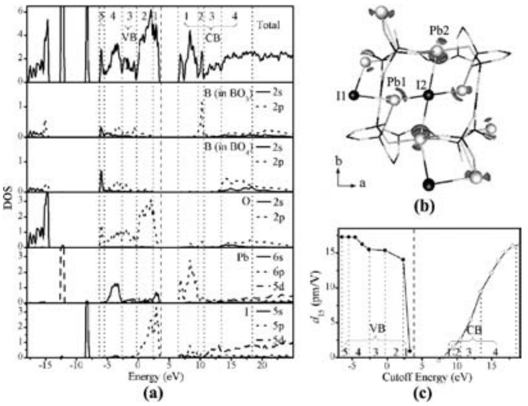

Figure 2. (a) Densities of states of $Pb_2B_5O_9I$. (b) Asymmetric electron distribution (>0.06 eV/Å^3) around Pb^{2+} at VB-1 region. (c) The cutoff-energy-dependent static SHG coefficients for $Pb_2B_5O_9I$, dashed line: E_F; dotted line: different regions in VB and CB.

In summary, a new phase-matchable compound $Pb_2B_5O_9I$ with the largest powder SHG coefficient among borates has been synthesized and characterized. Theoretical analyses reveal that the cooperation of I^-, lone pairs on Pb^{2+}, and the BO_3 and BO_4 groups are responsible for the remarkable SHG response. The growth of large crystals for further physical property studies is ongoing.

Acknowledgment. This research was supported by the National Natural Science Foundation of China under Projects (90922021, 90922022, 20773130, 20733003, 20821061, 20973175, 20773024), the "Knowledge Innovation Program of the Chinese Academy of Sciences" (KJCX2-YW-H20), and New Century Excellent Talents at Universities of Fujian Province (HX2006-97).

Supporting Information Available: The cif data, experimental and theoretical methods, and additional tables and figures. This material is available free of charge via the Internet at http://pubs.acs.org.

References

(1) Becker, P. *Adv. Mater.* **1998**, *10*, 979.
(2) Halasyamani, P. S. *Chem. Mater.* **2004**, *16*, 3586.
(3) Ok, K. M.; Halasyamani, P. S.; Casanova, D.; Llunell, M.; Alemany, P.; Alvarez, S. *Chem. Mater.* **2006**, *18*, 3176.
(4) Kim, S. H.; Yeon, J.; Halasyamani, P. S. *Chem. Mater.* **2009**, *21*, 5335.
(5) Kong, F.; Huang, S. P.; Sun, Z. M.; Mao, J. G.; Cheng, W. D. *J. Am. Chem. Soc.* **2006**, *128*, 7750.
(6) Ra, H. S.; Ok, K. M.; Halasyamani, P. S. *J. Am. Chem. Soc.* **2003**, *125*, 7764.
(7) Chang, H. Y.; Kim, S. H.; Halasyamani, P. S.; Ok, K. M. *J. Am. Chem. Soc.* **2009**, *131*, 2426.
(8) Zhang, W.-L.; Cheng, W.-D.; Zhang, H.; Geng, L.; Lin, C.-S.; He, Z.-Z. *J. Am. Chem. Soc.* **2010**, *132*, 1508.
(9) Inaguma, Y.; Yoshida, M.; Katsumata, T. *J. Am. Chem. Soc.* **2008**, *130*, 6704.
(10) Plachinda, P. A.; Dolgikh, V. A.; Stefanovich, S. Y.; Berdonosov, P. S. *Solid State Sci.* **2005**, *7*, 1194.
(11) Egorova, B. V.; Olenev, A. V.; Berdonosov, P. S.; Kuznetsov, A. N.; Stefanovich, S. Y.; Dolgikh, V. A.; Mahenthirarajah, T.; Lightfoot, P. *J. Solid State Chem.* **2008**, *181*, 1891.
(12) Belokoneva, E. L.; Al-Ama, A. G.; Stefanovich, S. Y.; Plachinda, P. A. *Crystallogr. Rep.* **2007**, *52*, 795.
(13) Rashkeev, S. N.; Lambrecht, W. R. L.; Segall, B. *Phys. Rev. B* **1998**, *57*, 3905.
(14) Aversa, C.; Sipe, J. E. *Phys. Rev. B* **1995**, *52*, 14636.
(15) Watson, G. W.; Parker, S. C. *J. Phys. Chem. B* **1999**, *103*, 1258.
(16) Payne, D. J.; Egdell, R. G.; Walsh, A.; Watson, G. W.; Guo, J.; Glans, P. A.; Learmonth, T.; Smith, K. E. *Phys. Rev. Lett.* **2006**, *96*, 157403.
(17) Seshadri, R.; Hill, N. A. *Chem. Mater.* **2001**, *13*, 2892.
(18) Stoltzfus, M. W.; Woodward, P. M.; Seshadri, R.; Klepeis, J.-H.; Bursten, B. *Inorg. Chem.* **2007**, *46*, 3839.

JA106066K